NMR Signatures and Electronic Structures of Ti-sites in Titanosilicalite-1 from solid-state $^{47/49}$Ti NMR Spectroscopy

Lukas Lätsch,[†] Imke B. Müller,[‡] Alia Hassan,[+] Barbara Perrone,[+] Sadig Aghazada,[†] Zachariah J. Berkson,[†] Alexander V. Yakimov,[†] Trees De Baerdemaeker,[‡] Andrei-Nicolae Parvulescu,[‡] Karsten Seidel,[‡] J. Henrique Teles,[‡] & Christophe Copéret[†,*]

[†]*ETH Zurich, Department of Chemistry and Applied Biosciences, Vladimir-Prelog Weg 2, Zurich, Switzerland*
[‡]*BASF SE, Ludwigshafen, Germany*
[+]*Bruker Switzerland, Fällanden, Switzerland*

ABSTRACT: Although titanosilicalite-1 (TS-1) is among the most successful oxidation catalysts used in industry, its active site structure is still debated. Recent efforts have mostly focused on understanding the role of defect sites and extra-framework Ti. Insights into the positions and distributions of framework tetrahedral Ti sites remain scarce, in part due to the lack of direct characterization techniques with sufficient sensitivity. Here, we report the $^{47/49}$Ti solid-state NMR characterization of TS-1 and its molecular models, [Ti(OTBOS)$_4$] and [Ti(OTBOS)$_3$(O^{i}Pr)]. Analysis of their spectroscopic signatures, augmented by computational studies, shows pronounced differences that originate from specific arrangements of the second coordination sphere of Ti atoms, yielding information on titanium siting in TS-1.

Titanosilicates are important class of heterogenous catalysts where Ti is typically incorporated into the crystalline lattice of a zeolite-type framework.[1] The discovery of titanosilicalite-1 (TS-1) *ca.* 40 years ago has enabled the development of sustainable processes based on H_2O_2 as a primary oxidant, leaving H_2O as the sole byproduct.[2] Notable industrial examples are the hydroxylation of phenol,[3] the epoxidation of propylene[4] and the ammoximation of ketones.[5-6] TS-1 has been proposed to contain isolated framework tetrahedral Ti sites, generated by substitution of a small fraction of Si atoms in the zeolite structure.[7] Note that the coordination environment of Ti can be dramatically influenced by the preparation method and the state of the catalysts; such sites include partially hydrolyzed octahedral sites,[8] penta-coordinated sites,[9] tetrahedral titanols[10], and octahedral defect sites.[11] Recently, paired Ti sites have been observed upon activation with H_2O_2.[12]

The coordination environment in titanosilicates has been addressed by direct and indirect characterization methods. The latter relies on using probe molecules such as phosphines [13] or pyridine[14] as well as reactants, e.g. H_2O_2[12] in combination with IR and/or solid-state nuclear magnetic resonance (ssNMR) spectroscopies. Direct approaches have focused on UV/Vis, Raman and X-Ray Absorption Spectroscopy (K and $L_{2,3}$ edge XANES).[11,15] Even though these techniques can provide information on

the extent of Ti incorporation into the framework or the ratio between tetrahedral to octahedral Ti sites, they are limited to averaged local structural information and rely mostly on empirical interpretation. In addition, information on preferential Ti siting at different tetrahedral (T) positions can be obtained from neutron powder diffraction (NPD) analysis but the interpretation is often complicated by the difficulty to distinguish between Ti-sites and silicon vacancies.[16–19]

$^{47/49}$Ti ssNMR spectroscopy could be an alternative direct characterization method to access non-averaged information on the local coordination geometry of Ti.[20–22] Titanium possesses two NMR-active nuclei, ^{47}Ti (I =5/2) and ^{49}Ti (I =7/2), which are both commonly termed as 'unreceptive' due to their low natural abundances (7.44% for ^{47}Ti and 5.41% for ^{49}Ti), moderate quadrupole moments ($Q(^{47}Ti)$ = 29.0 fm^2 and $Q(^{49}Ti)$ = 24.0 fm^2) and low gyromagnetic ratios ($\gamma(^{47}Ti) = -1.5105 \cdot 10^7$ rad s^{-1} T^{-1}, $\gamma(^{49}Ti) = -1.51095 \cdot 10^7$ rad s^{-1} T^{-1}).[23] Due to close gyromagnetic ratios, NMR signals from ^{47}Ti and ^{49}Ti usually overlap, which further complicates analysis.[24] To this date, $^{47/49}$Ti ssNMR spectroscopy has been mostly limited to the investigation of bulk materials such as titanium oxides and carbides.[25–27] One notable exception is the characterization of titanocene chlorides, demonstrating the sensitivity of $^{47/49}$Ti ssNMR parameters to local structure.[24,28] The scope of $^{47/49}$Ti ssNMR has since been expanded through the development of novel pulse sequences and/or the use of dynamic nuclear polarization surface-enhanced NMR spectroscopy (DNS-SENS),[29] which has enabled the detection of Ti surface signals in hydrated TiO_2-supported MoO_3, albeit necessitating a very high concentration of polarizing agent. So far, ssNMR spectroscopy of low-γ quadrupolar nuclei such as $^{47/49}$Ti is remains challenging for samples with low Ti loadings (few wt%) or containing Ti with large C_Q (e.g. > 15 MHz).

Here, we report the $^{47/49}$Ti ssNMR signatures of a typical titanosilicate-1 catalyst (1.5 wt% Ti) and their relation to the electronic structure of Ti sites obtained from analysis of related solid-state Ti-oxides anatase and rutile, and molecular compounds – $[Ti(OTBOS)_4]$ (OTBOS = *tris*(*tert*-butoxy)siloxy) and $[Ti(OTBOS)_3(O^iPr)]$. The measurements were enabled by the recent development of a low-γ solid-state NMR probe with cryogenic cooling of electronic components (CryoProbe^{TM} with thermally decoupled sample temperature) for a B_0 field of 18.8 T, which significantly boosts NMR signal sensitivity under both static and magic angle spinning (MAS) conditions.[30] In particular, the use of MAS enables resolution of ^{47}Ti and ^{49}Ti NMR signals. Comparison of the NMR signatures of Ti in TS-1 and in its molecular homologues, augmented with computational studies, shows pronounced differences that originate from the specific arrangement of the second coordination sphere of Ti, characteristic of specific T-site positions of the MFI framework.

To evaluate the sensitivity of the CryoProbe^{TM}, ssNMR spectra of anatase TiO_2 (60 wt% Ti) were recorded under static (WURST-QCMPG)[31] and MAS (DFS-QCPMG-MAS) conditions.[32,33] The

sensitivity was compared to measurements performed with a low temperature probe at 14.1 T, available in our laboratory, where the sample rests at ca. 100 K (ESI Fig. S1). Calculated signal-to-noise ratios indicate that the CryoProbe^{TM} provides sensitivity enhancement factors of 10–15, arising from cryogenic cooling of the RF coil and preamplifier electronics (~4x)[34], as well as a larger active sample volume (~3x) owing to longer rotors that the Cryo-Probe^{TM} uses. The sensitivity gain from the higher field (18.8 T) is roughly compensated with low temperature measurements at 14.1 T (100 K). Note that the gain from signal narrowing is sample dependent. Notably, as anatase shows a reasonably small C_Q (~5 MHz), its ^{47}Ti and ^{49}Ti signals can be resolved under MAS. This enables a more facile interpretation of the spectroscopic signature than under static conditions (Figure 1). For rutile, which is associated with larger C_Q, signals up to 5000 ppm wide can be recorded without the need for multiple offsets and spectrum reconstruction (ESI Fig. S2).

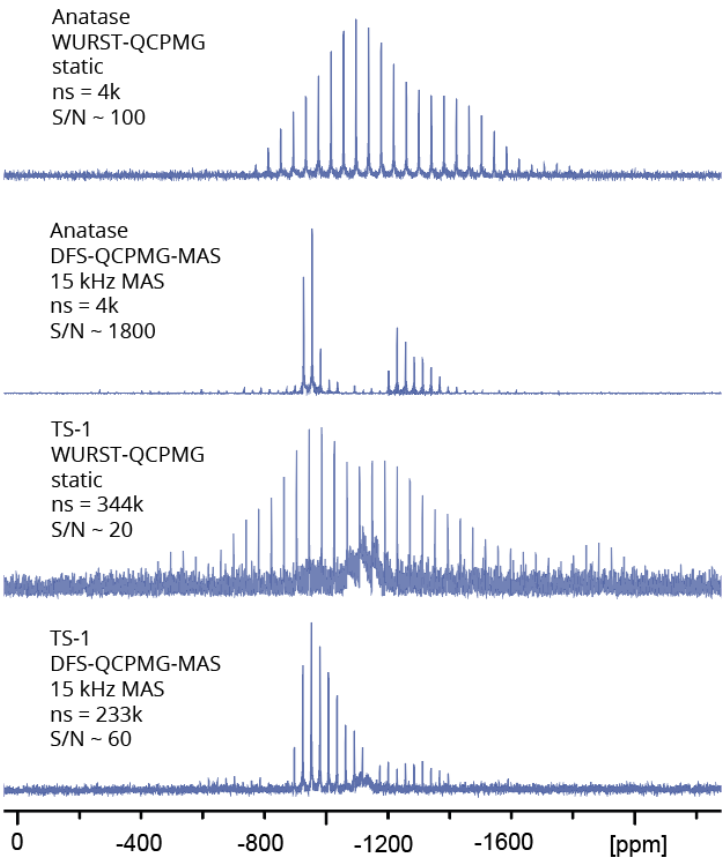

Figure 1: DFS-QCPMG-MAS (15kHz) and WURST-QCPMG spectra of anatase (top) and TS-1 (bottom) acquired at 298 K, 18.8 T (ns = number of scans, S/N = signal-to-noise ratio).

Having obtained encouraging preliminary results, we focused on more challenging materials such as TS-1, with low Ti wt%-loading (here, 1.5 w%). Both static and MAS spectra were recorded with good signal-to-noise ratios in reasonable times (see Fig. 1, S/N_{static}=21, t=3 days and S/N_{MAS}=65, t=1 day).

NMR parameters extracted from the static and MAS spectra according to the Czjzek model[35] show an isotropic chemical shift (δ_{iso}) of –940 ppm for ^{49}Ti and a characteristic C_Q of 8.0 MHz, consistent with an all oxygen tetrahedral first coordination sphere (*vide infra*). Notably, no signal is observed in the corresponding hydrated TS-1 sample, likely due to the formation of highly distorted Ti sites with very large C_Q values (> 25 MHz as indicated by DFT calculations, ESI Fig. S3), upon hydration (coordination or reaction with water). This is consistent with pXRD[36] and XAS data, the latter showing a sharp decrease of the pre-edge feature specific of tetrahedral sites upon water adsorption (ESI Fig. S4).

Given the response of $^{47/49}$Ti NMR signatures to subtle changes in coordination environment,[24] we next evaluated two tetrahedral molecular complexes. As molecular models for TS-1, [Ti(OTBOS)$_4$] and [Ti(OTBOS)$_3$(O^{i}Pr)] were selected, having only oxygens in the first coordination sphere (see SI for synthesis and analysis).[37,38] According to single crystal X-Ray Diffraction (XRD) analysis, both molecular models possess near perfect tetrahedral geometries, as illustrated by their τ_4' values equal to 0.99.[38,39] Homoleptic [Ti(OTBOS)$_4$] features four chrystallographically identical Ti−OSi bonds (1.785 Å), while in the heteroleptic [Ti(OTBOS)$_3$(O^{i}Pr)], the Ti−OSi bonds are slightly elongated (1.795 Å) and the Ti−O^{i}Pr bond is slightly shortened (1.748 Å). Notably, while these compounds, [Ti(OTBOS)$_4$], [Ti(OTBOS)$_3$(O^{i}Pr)], show a pre-edge feature in Ti K edge XANES spectra typical for tetrahedral complexes, with position and intensity similar to TS-1 (ESI Fig. S6), their NMR signatures are significantly different from each other and that of TS-1.[40] While the Ti sites of TS-1 appear at δ_{iso} = –940 ppm for ^{49}Ti, it is more deshielded for [Ti(OTBOS)$_4$] (δ_{iso} = –919 ppm) and even further deshielded for [Ti(OTBOS)$_3$(O^{i}Pr)] (δ_{iso} = –895 ppm for ^{49}Ti). This difference in δ_{iso} is also accompanied by a significant difference in C_Q values of 2.3 MHz for [Ti(OTBOS)$_4$] and 4.0 MHz for [Ti(OTBOS)$_3$(O^{i}Pr)], consistent with the asymmetry in the Ti−O bond lengths for the heteroleptic complex. Intriguingly, although TS-1 shows a highly symmetric first coordination sphere, the observed C_Q of TS-1 (8.0 MHz) is significantly larger than for both molecular models.

To systematically study the origin of the observed changes, we computed the NMR parameters for a series of four-coordinated [Ti(OX)$_4$] models (X = OCH_3, $OSiF_3$ and OCF_3). All compounds show tetrahedral geometry with different Ti−O−X bond angles, with the [Ti($OSiF_3$)$_4$] displaying more linear bond angles (167°) than [Ti(OCF_3)$_4$] (158°) and [Ti(OCH_3)$_4$] (153°). Calculated chemical shifts (see ESI for computational details) for the series are referenced with respect to [Ti(OTBOS)$_4$] (δ_{iso} = -919 ppm, $\Delta\delta_{iso}$ = 0 ppm) and show gradual shielding for more electron withdrawing ligands:[41] [Ti(OCH_3)$_4$] ($\Delta\delta_{iso}$ = +31 ppm), [Ti($OSiF_3$)$_4$] ($\Delta\delta_{iso}$ = -30 ppm) and [Ti(OCF_3)$_4$] (-117 ppm). The agreement between the experimentally observed ($\Delta\delta_{iso}$ = +24 ppm) and the calculated ($\Delta\delta_{iso}$ = +18 ppm (calc.)) chemical shift for [Ti(OTBOS)$_3$(O^{i}Pr)] in reference to [Ti(OTBOS)$_4$] substantiates the analysis based on model systems.

The good match between the [Ti(OSiF$_3$)$_4$] model ($\Delta\delta_{iso}$ = –30 ppm) and the experimentally observed chemical shift for TS-1 confirms the higher electron withdrawing character of the silicate framework compared to the OTBOS ligand.

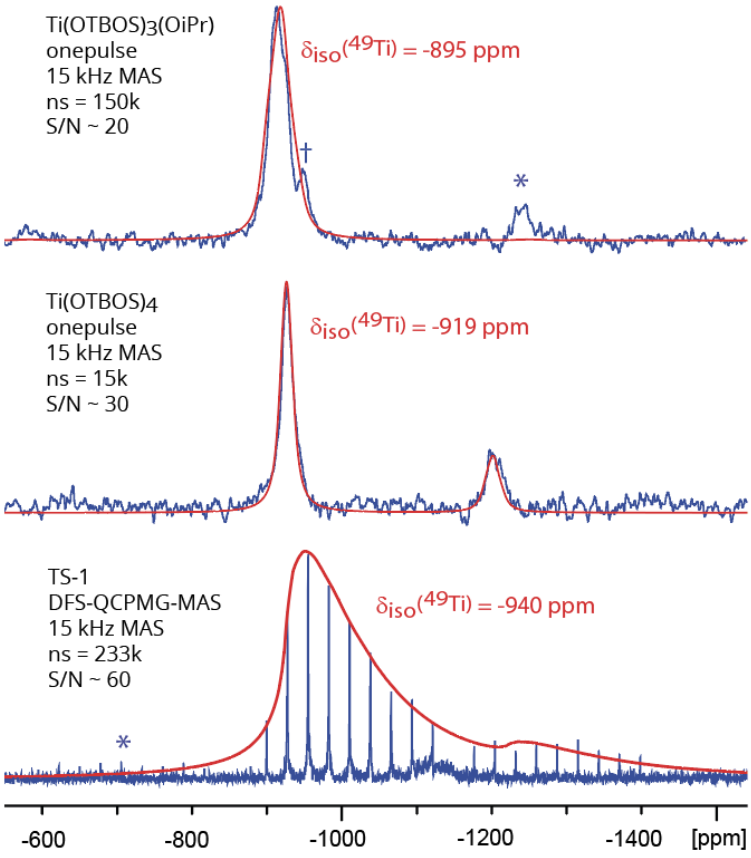

Figure 2: Direct excitation spectra (blue) of [Ti(OTBOS)$_3$(O^{i}Pr)] (top, ^{47}Ti not observed) and [Ti(OTBOS)$_4$] (middle), as well as DFS-QCPMG-MAS spectrum of TS-1 (bottom) all acquired at RT, 18.8 T and 15 kHz MAS, with corresponding lineshape simulations (red). * denotes spinning side bands and † an artefact due to direct excitation and signal processing.

We next traced back the origin of the chemical shift differences using Natural Chemical Shift (NCS)-analysis that allows the determination of the relative magnetic couplings between occupied and vacant orbitals of appropriate symmetries responsible for paramagnetic deshielding.[42,43] Here, the dominant couplings arise from the σ(Ti–O) and π(Ti–O) frontier orbitals (see Fig. 3a). Higher ligand electronegativity leads to shielding as the energy gap between the filled σ(Ti–O) and the empty π*(Ti–O) is raised (*cf.* [Ti(OCH$_3$)$_4$] vs. [Ti(OCF$_3$)$_4$]). Shielding can also arise from a more linear Ti-O-X arrangement, as the higher electron delocalization may stabilize the π(Ti–O)-bonds (*cf.* [Ti(OCH$_3$)$_4$] vs. [Ti(OSiF$_3$)$_4$] & [Ti(OTBOS)$_3$(O^{i}Pr)] vs. [Ti(OTBOS)$_4$]).

Apart from the isotropic chemical shift difference between TS-1 and the molecular models, the

significantly larger C_Q for TS-1 (8.0 MHz) than for [Ti(OTBOS)$_4$] (2.3 MHz) is also noteworthy. Quadrupolar couplings are particularly sensitive to small changes in coordination environment, usually associated with the first coordination sphere (as the pre-edge Ti K edge XANES), but can also relate to the second coordination sphere (*vide infra*), hence providing information on the location of Ti in specific T-site positions, making NMR a complementary technique to neutron diffraction studies.[16,19] Hence, we calculated the NMR parameter for all twelve T-sites in TS-1 by extracting cluster models terminated by fluorine atoms and obtained by isomorphous substitution of Si with Ti in the respective T-Site of the MFI structure (see ESI for details). Overall, C_Q values vary between 3.6 MHz and 9.5 MHz (see Fig. 3b). The experimental $^{47/49}$Ti NMR parameters obtained for TS-1 match best with computed parameters for T2, T6 and T7 positions, which is in partial agreement with previous neutron diffraction studies.[19] These large differences for the various T-sites must arise from the specific electronic structures and local geometries that affects C_Q. While all T-sites show near perfect tetrahedral geometry in the first coordination sphere (τ_4' = 0.99) consistent with Ti K edge XAS, the main variation in C_Q arises from the second coordination sphere, more specifically the average Si-Ti-Si angle as shown in Fig. 3c, with T7 having a remarkably large C_Q because of the significantly larger average O-Ti-O-Si dihedral angle by comparison with other T-sites. Notably, the chemical shift of the T-sites correlates linearly with the average Ti-O-Si angle (ESI Fig. S9), in line with recent NMR studies.[44,45]

In conclusion, we obtained the $^{47/49}$Ti ssNMR signatures of TS-1, despite the low Ti loading (< 2 wt%). Comparison to molecular model complexes reveals that TS-1 shows both a more shielded chemical shift and a larger quadrupolar coupling. The lower isotropic chemical shift indicates a higher electron-withdrawing character of the MFI-type silicate framework than of the siloxide-ligand (OTBOS), and the difference in quadrupolar coupling could be traced back to differences in the second coordination sphere, namely the average Si-Ti-Si angle. As this angle is characteristic of specific T-sites, $^{47/49}$Ti NMR of TS-1 provides access to the location of Ti in specific T-sites, namely T2, T6, and T7; information that can otherwise only (partly) be obtained by NPD studies. Overall, this study highlights the advantages of direct characterization of the metal sites without probe molecule and opens the possibility to investigate other titanosilicates with differing framework architecture in order to evaluate the precise coordination environment and electronic structure of the respective active sites.

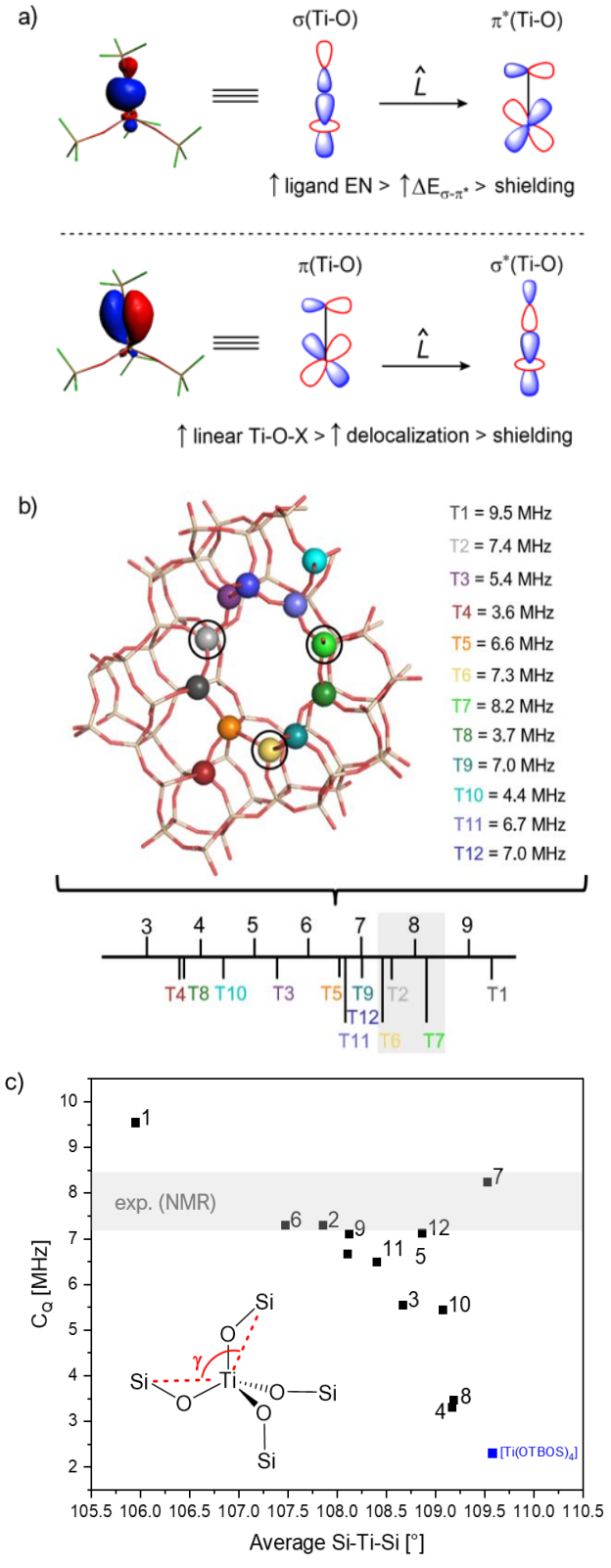

Figure 3: a) Relevant magnetic couplings that give rise to deshielding in the systems studied herein. b) Graphical illustration of the 12 T-Sites of the MFI-framework, their calculated C_Q values and linear scale representation. c) C_Q as a function of the average Si-Ti-Si angle. T-sites with a more tetrahedral 2nd coordination sphere (109.5°) are expected to have smaller C_Q.

ASSOCIATED CONTENT

CCDC 2205478 contains the supplementary crystallographic data for this paper and can be obtained free of charge via www.ccdc.cam.ac.uk/data_request/cif, or by emailing data_request@ccdc.cam.ac.uk, or by contacting The Cambridge Crystallographic Data Centre, 12 Union Road, Cambridge CB2 1EZ, UK; fax: +44 1223 336033.

AUTHOR INFORMATION

Corresponding Author

* Christophe Copéret: ccoperet@ethz.ch.

CONFLICT OF INTEREST

A.H and B.P. are employed by the manufacturer of the NMR equipment used.

ACKNOWLEDGMENT

L.L. thanks the Scholarship Fund of the Swiss Chemical Industry (SSCI) and BASF for funding. A.Y. and Z.B. are grateful for SynMatLab for funding. S.A. acknowledges a fellowship from the Swiss National Science Foundation (P5R5PN_202658). We thank Dr. D. Nater for assistance with the XRD measurements. Recording of XRD powder diffractograms by Dirk Paulus and Murat Yavuz (BASF SE, Ludwigshafen) is kindly acknowledged. The Swiss Norwegian beamlines (SNBL, ESRF) are acknowledged for provision of beamtime through proposal 31-01-143. We thank Dr. W. van Beek and Dr. D. Stoian for their support during XAS experiments.

REFERENCES

(1) Smeets, V.; Gaigneaux, E. M.; Debecker, D. P. Titanosilicate Epoxidation Catalysts: A Review of Challenges and Opportunities. *ChemCatChem* **2022**, *14* (1), 1–26.

(2) Xu, H.; Wu, P. Recent Progresses in Titanosilicates. *Chinese J. Chem.* **2017**, *35* (6), 836–844.

(3) Romano, U.; Esposito, A.; Maspero, F.; Neri, C.; Clerici, G. M. *Selective oxidation with Ti-silicalite*. Chim.Ind.(Milan). 1990, p 610-616.

(4) Lin, M.; Xia, C.; Zhu, B.; Li, H.; Shu, X. Green and Efficient Epoxidation of Propylene with Hydrogen Peroxide (HPPO Process) Catalyzed by Hollow TS-1 Zeolite: A 1.0 Kt/a Pilot-Scale Study. *Chem. Eng. J. (Amsterdam, Neth.)* **2016**, *295*, 370–375.

(5) Ge, Q.; Lu, J.; Zhu, M. *Research Progress of Titanium Silicalite Molecular Sieve for Cyclohexanone Ammoximation*; Hecheng Xianwei Gongye: 38(1), 54-58, 2015.

(6) Li, M.; Liu, J.; Na, H. *Application and Advancements in Synthesis of 2-Butanone Oxime*; Huaxue Gongchengshi: 20(7), 42-43, 2006.

(7) Taramasso, M.; Perego, G.; Notari, B. *US4410501A*; 1983.

(8) Guo, Q.; Sun, K.; Feng, Z.; Li, G.; Guo, M.; Fan, F.; Li, C. A Thorough Investigation of the Active Titanium Species in TS-1 Zeolite by in Situ UV Resonance Raman Spectroscopy. *Chem. - A Eur. J.* **2012**, *18* (43), 13854–13860.

(9) Zuo, Y.; Liu, M.; Zhang, T.; Hong, L.; Guo, X.; Song, C.; Chen, Y.; Zhu, P.; Jaye, C.; Fischer, D. Role of Pentahedrally Coordinated Titanium in Titanium Silicalite-1 in Propene Epoxidation. *RSC Adv.* **2015**, *5* (23), 17897–17904.

(10) Wang, J.; Chen, Z.; Yu, Y.; Tang, Z.; Shen, K.; Wang, R.; Liu, H.; Huang, X.; Liu, Y. Hollow Core-Shell Structured TS-1@S-1 as an Efficient Catalyst for Alkene Epoxidation. *RSC Adv.* **2019**, *9* (65), 37801–37808.

(11) Signorile, M.; Braglia, L.; Crocellà, V.; Torelli, P.; Groppo, E.; Ricchiardi, G.; Bordiga, S.; Bonino, F. Titanium Defective Sites in TS-1: Structural Insights by Combining Spectroscopy and Simulation. *Angew. Chemie - Int. Ed.* **2020**, *59* (41), 18145–18150.

(12) Gordon, C. P.; Engler, H.; Tragl, A. S.; Plodinec, M.; Lunkenbein, T.; Berkessel, A.; Teles, J. H.; Parvulescu, A. N.; Copéret, C. Efficient Epoxidation over Dinuclear Sites in Titanium Silicalite-1. *Nature* **2020**, *586* (7831), 708–713.

(13) Zhuang, J.; Yan, Z.; Liu, X.; Liu, X.; Han, X.; Bao, X.; Mueller, U. NMR Study on the Acidity of TS-1 Zeolite. *Catal. Letters* **2002**, *83* (1–2), 87–91.
(14) Gunther, W. R.; Michaelis, V. K.; Griffin, R. G.; Roman-Leshkov, Y. Interrogating the Lewis Acidity of Metal Sites in Beta Zeolites with ^{15}N Pyridine Adsorption Coupled with MAS NMR Spectroscopy. *J. Phys. Chem. C* **2016**, *120* (50), 28533–28544.
(15) Spanjers, C. S.; Guillo, P.; Tilley, T. D.; Janik, M. J.; Rioux, R. M. Identification of Second Shell Coordination in Transition Metal Species Using Theoretical XANES: Example of Ti-O-(C, Si, Ge) Complexes. *J. Phys. Chem. A* **2017**, *121* (1), 162–167.
(16) Henry, P. F.; Weller, M. T.; Wilson, C. C. Structural Investigation of TS-1: Determination of the True Nonrandom Titanium Framework Substitution and Silicon Vacancy Distribution from Powder Neutron Diffraction Studies Using Isotopes. *J. Phys. Chem. B* **2001**, *105* (31), 7452–7458.
(17) Dong, J.; Zhu, H.; Xiang, Y.; Wang, Y.; An, P.; Gong, Y.; Liang, Y.; Qiu, L.; Zheng, A.; Peng, X.; Lin, M.; Xu, G.; Guo, Z.; Chen, D. Toward a Unified Identification of Ti Location in the MFI Framework of High-Ti-Loaded TS-1: Combined EXAFS, XANES, and DFT Study. *J. Phys. Chem. C* **2016**, *120* (36), 20114–20124.
(18) Hijar, C. A.; Jacubinas, R. M.; Eckert, J.; Henson, N. J.; Hay, P. J.; Ott, K. C. The Siting of Ti in TS-1 Is Non-Random. Powder Neutron Diffraction Studies and Theoretical Calculations of TS-1 and FeS-1. *J. Phys. Chem. B* **2000**, *104* (51), 12157–12164.
(19) Lamberti, C.; Bordiga, S.; Zecchina, A.; Artioli, G.; Marra, G.; Spanò, G. Ti Location in the MFI Framework of Ti-Silicalite-1: A Neutron Powder Diffraction Study. *J. Am. Chem. Soc.* **2001**, *123* (10), 2204–2212.
(20) Lucier, B. E. G.; Huang, Y. *Reviewing 47/49 Solid-State NMR Spectroscopy: From Alloys and Simple Compounds to Catalysts and Porous Materials*, 1st ed.; Elsevier Ltd., 2016; Vol. 88.
(21) Ganapathy, S.; Gore, K. U.; Kumar, R.; Amoureux, J. P. Multinuclear (^{27}Al, ^{29}Si, ^{47,49}Ti) Solid-State NMR of Titanium Substituted Zeolite USY. *Solid State Nucl. Magn. Reson.* **2003**, *24* (2-3 SPEC.), 184–195..
(22) Lopez, A.; Tuilier, M. H.; Guth, J. L.; Delmotte, L.; Popa, J. M. Titanium in MFI-Type Zeolites: A Characterization by XANES, EXAFS, IR, and $^{74,\ 49}$Ti and ^{17}O MAS NMR Spectroscopy and H2O Adsorption. *J. of Solid State Chem.* **1993**, pp 480–491.
(23) Harris, R. K.; Becker, E. D.; Cabral de Menezes, S. M.; Goodfellow, R.; Granger, P. NMR Nomenclature. Nuclear Spin Properties and Conventions for Chemical Shifts (IUPAC Recommendations 2001). *Pure Appl. Chem.* **2001**, *73* (11), 1795–1818.
(24) Rossini, A. J.; Hung, I.; Schurko, R. W. Solid-State $^{47/49}$Ti NMR of Titanocene Chlorides. *J. Phys. Chem. Lett.* **2010**, *1* (20), 2989–2998.
(25) Stephens, K. J.; Zichittella, G.; Saadun, A. J.; Büchele, S.; Puértolas, B.; Verel, R.; Verel, R.; Krumeich, F.; Willinger, M. G.; Pérez-Ramírez, J. Transformation of Titanium Carbide into Mesoporous Titania for Catalysed HBr Oxidation. *Catal. Sci. Technol.* **2020**, *10* (12), 4072–4083.
(26) Gervais, C.; Smith, M. E.; Pottier, A.; Jolivet, J. P.; Babonneau, F. Solid-State ^{47,49}Ti MNR Determination of the Phase Distribution of Titania Nanoparticles. *Chem. Mater.* **2001**, *13* (2), 462–467.
(27) Larsen, F. H.; Farnan, I.; Lipton, A. S. Separation of ^{47}Ti and ^{49}Ti Solid-State NMR Lineshapes by Static QCPMG Experiments at Multiple Fields. *J. Magn. Reson.* **2006**, *178* (2), 228–236.
(28) For example, the spectroscopic signatures of $CpTiCl_3$ and Cp^*TiCl_3 showed an increased chemical shift anisotropy (CSA) by >500 ppm upon replacing the protons of the cyclopentadienyl (Cp) ligand by methyl groups (Cp*). Measurement of these molecular complexes was however only possible because of their pseudo-tetrahedral geometry, yielding relatively small quadrupolar coupling constants ($C_Q < 6$ MHz).
(29) Nagashima, H.; Trébosc, J.; Trébosc, J.; Kon, Y.; Sato, K.; Lafon, O.; Lafon, O.; Amoureux, J. P.; Amoureux, J. P.; Amoureux, J. P. Observation of Low-γ Quadrupolar Nuclei by Surface-Enhanced NMR Spectroscopy. *J. Am. Chem. Soc.* **2020**, *142* (24), 10659–10672.
(30) Hassan, A.; Quinn, C. M.; Struppe, J.; Sergeyev, I. V.; Zhang, C.; Guo, C.; Runge, B.; Theint, T.; Dao, H. H.; Jaroniec, C. P.; Berbon, M.; Lends, A.; Habenstein, B.; Loquet, A.; Kuemmerle, R.; Perrone, B.; Gronenborn, A. M.; Polenova, T. Sensitivity Boosts by the CPMAS CryoProbe for Challenging Biological Assemblies. *J. Magn. Reson.* **2020**, *311*, 106680.
(31) Schurko, R. W. Ultra-Wideline Solid-State NMR Spectroscopy. *Acc. Chem. Res.* **2013**, *46* (9), 1985–1995.
(32) Iuga, D.; Schäfer, H.; Verhagen, R.; Kentgens, A. P. M. Population and Coherence Transfer Induced by Double Frequency Sweeps in Half-Integer Quadrupolar Spin Systems. *J. Magn. Reson.* **2000**, *147* (2), 192–209.

(33) Larsen, F. H.; Jakobsen, H. J.; Ellis, P. D.; Nielsen, N. C. QCPMG-MAS NMR of Half-Integer Quadrupolar Nuclei. *J. Magn. Reson.* **1998**, *131* (1), 144–147.
(34) Styles, P.; Soffe, N. F.; Scott, C. A.; Cragg, D. A.; Row, F.; White, D. J.; White, P. C. J. A High-Resolution NMR Probe in Which the Coil and Preamplifier Are Cooled with Liquid Helium. *J. Magn. Reson.* **2011**, *213* (2), 347–354.
(35) d'Espinose de Lacaillerie, J. B.; Fretigny, C.; Massiot, D. MAS NMR Spectra of Quadrupolar Nuclei in Disordered Solids: The Czjzek Model. *J. Magn. Reson.* **2008**, *192* (2), 244–251.
(36) Note that powder X-ray diffraction of the hydrated and dehydrated samples (for details see ESI Fig. S5.) show no sizeable difference, indicating that water coordination to Ti is the primary reason for the observed signal loss.
(37) Coles, M. P.; Lugmair, C. G.; Terry, K. W.; Tilley, T. D. Titania-Silica Materials from the Molecular Precursor $Ti[OSi(O^tBu)_3]_4$: Selective Epoxidation Catalysts. *Chem. Mater.* **2000**, *12* (1), 122–131.
(38) Noh, G.; Lam, E.; Alfke, J. L.; Larmier, K.; Searles, K.; Wolf, P.; Copéret, C. Selective Hydrogenation of CO_2 to CH_3OH on Supported Cu Nanoparticles Promoted by Isolated Ti^{IV} Surface Sites on SiO_2. *ChemSusChem* **2019**, *12* (5), 968–972.
(39) Okuniewski, A.; Rosiak, D.; Chojnacki, J.; Becker, B. Coordination Polymers and Molecular Structures among Complexes of Mercury(II) Halides with Selected 1-Benzoylthioureas. *Polyhedron* **2015**, *90*, 47–57.
(40) Because of their very small C_Qs CPMG acquisition could not be applied without signal truncation and due to the low Ti w% contents as the result of using the large siloxide ligands ($Ti(OTBOS)_4$: 4.4 w% Ti and $Ti(OTBOS)_3(OiPr)$: 5.3 w% Ti) only MAS spectra were recorded.
(41) Feige, F.; Malaspina, L. A.; Rychagova, E.; Ketkov, S.; Grabowsky, S.; Hupf, E.; Beckmann, J. Perfluorinated Trialkoxysilanol with Dramatically Increased Brønsted Acidity. *Chem. - A Eur. J.* **2021**, *27* (64), 15898–15902.
(42) Gordon, C. P.; Lätsch, L.; Copéret, C. Nuclear Magnetic Resonance: A Spectroscopic Probe to Understand the Electronic Structure and Reactivity of Molecules and Materials. *J. Phys. Chem. Lett.* **2021**, *12* (8), 2072–2085.
(43) Ramsey, N. F. Magnetic Shielding of Nuclei in Molecules. *Phys. Rev.* **1950**, *78* (6), 699–703.
(44) Berkson, Z. J.; Lätsch, L.; Hillenbrand, J.; Fürstner, A.; Copéret, C. Classifying and Understanding the Reactivities of Mo-Based Alkyne Metathesis Catalysts from ^{95}Mo NMR Chemical Shift Descriptors. *J. Am. Chem. Soc.* **2022**, *144* (33), 15020–15025.
(45) Dawson, D. M.; Moran, R. F.; Ashbrook, S. E. An NMR Crystallographic Investigation of the Relationships between the Crystal Structure and ^{29}Si Isotropic Chemical Shift in Silica Zeolites. *J. Phys. Chem. C* **2017**, *121* (28), 15198–15210.